JOURNAL OF APPLIED ELECTROCHEMISTRY 20 (1990) 381–389

On the nature of the 'induction period' during the electrowinning of zinc from nickel containing sulphate electrolytes*

R. WIART, C. CACHET

LP15 du CNRS Physique des Liquides et Electrochimie Laboratoire de l'Université Pierre et Marie Curie, Tour 22, 4 place Jussieu, 75252 Paris Cedex 05, France

CHR. BOZHKOV‡, ST. RASHKOV

Institute of Physical Chemistry, Bulgarian Academy of Sciences, Sofia 1040, Bulgaria

Received 10 February 1989; revised 27 June 1989

As a result of detailed voltammetric, impedance, electron microscopic and optical *in situ* investigations of the peculiarities encountered in zinc electrowinning from nickel-containing acid electrolytes, a model for the 'induction period' is proposed and its dependence on the process conditions is elucidated. The model is based on the screening effect of hydrogen bubbles formed on the nickel-rich regions of the cathode which give rise to local galvanic cells.

Nomenclature

C	electrode capacitance
C_{dl}	double layer capacitance
C_{Ni}	volume concentration of Ni^{2+} ions
d	diameter of the circle along which the hydrogen bubble is attached to the surface
D_{Ni}	diffusion coefficient of Ni^{2+} ion
E_{zc}	potential of zero charge
f^*	frequency at the apex of the capacitance loop
F	Faraday constant
F_c	capillary force
F_h	hydrostatic force
g	acceleration due to gravity
q	specific mass of the liquid
h	height of the hydrogen bubble
R	electrolyte resistance
R_t	charge transfer resistance
V	volume of the gas phase
δ	thickness of the diffusion layer
θ	wetting angle at the metal-solution-gas interface
σ_{12}, σ_{23}, σ_{13}	surface tensions between: solid-liquid, liquid-gas and solid-gas phases, respectively
ν	kinematic viscosity
ω	rotation speed of the cathode

1. Introduction

The term 'induction period' of the electrowinning process is widely used in the literature and in the practice of zinc electroextraction from acidic sulphate electrolytes, containing metal impurities [1–5]. During this time period, which coincides with the beginning of the process, the zinc deposits are uniform, light coloured and adhere firmly to the cathode; the typical mean current yield of zinc reaches 93–95%. Following this period a characteristic spontaneous 'self-dissolution' of the zinc deposit occurs with hydrogen evolution leading to the formation of a sulphuric acid mist and a loss of energy efficiency. After the zinc is completely dissolved down to the aluminium cathode, deposition restarts. The sequence of this cycle (deposition – dissolution) can occur several times during a 24 h run.

It has been established that the duration of the 'induction period' depends on several factors. For example, temperature, electrolyte acidity, cathodic current density, concentration of metal impurities and concentration of zinc salt [4, 6]. According to some authors [7, 8], these relationships unambiguously render the phenomenon dependent on the conditions which control the rate of the simultaneously proceeding electrochemical discharge of hydrogen ions. However the phenomena which produce the 'induction period' are not yet elucidated. Consider:

(a) The explanation of the effect exerted by more positive metal impurities, widely accepted in the literature, is based on the 'local pairs' model [2, 5, 7–10]. According to this model, the metal impurity codeposited with zinc behaves as a cathode with respect to the zinc deposit and catalyses the hydrogen discharge reaction. But this model is unable to predict any time

* The first results were presented at the International Conference on 'Base Metals Technology', 8–10 February, 1989, Jamshedpur, India.
‡ To whom correspondence should be addressed.

0021-891X/90 $03.00 + .12 © 1990 Chapman and Hall Ltd.

dependence of the negative effect of metal impurities and, thus, cannot explain the presence of the 'induction period'. In addition, the 'local pairs' model is common for all electropositive metal impurities (nickel, cobalt, copper, germanium, arsenic, antimony, etc. . .) whereas 'induction periods' are observed only in the presence of iron-group metal impurities.

(b) It has been shown [5] that small amounts of Ni^{2+} ($10\,mg\,l^{-1}$) do not change the structural characteristics (preferred orientation, grain size, deposit morphology) of zinc deposits obtained for 1 h deposition, thus suggesting that the reasons leading to the 'self-dissolution' of zinc deposits do not display a clear-cut structural nature.

(c) It has also been established that the duration of the 'induction period' depends strongly on the moment when the metal impurities appear in the processed solutions. It has been shown that when a zinc substrate is used, its duration is 5–6 times longer as compared with the case when an aluminium cathode is used [11, 12]. Therefore, the nature of the electrode-substrate should also be taken into consideration.

Given these considerations this paper aims to gain more insight into the physical nature of the 'induction period' by performing both kinetic and structural investigations for zinc electrowinning in the presence of nickel in the electrolyte.

2. Experimental details

The electrochemical measurements were carried out in a thermostated three-electrode cell with a volume of 250 ml. The cathode, was a rotating disc electrode made of a 5 mm diameter aluminium rod (Johnson Matthey). The anode was a platinum mesh with an overall area of $100\,cm^2$. The reference was a mercury sulphate electrode. The cathode was rotated between $\omega = 0$–2500 rpm. The temperature during the investigation was 37° C and the pH was 0.2.

The base electrolyte had the following composition in $g\,l^{-1}$: H_2SO_4 – 130; $MnSO_4.H_2O$ – 15.5; $ZnSO_4.7H_2O$ – 220. To the base electrolyte was added $NiSO_4$, so that the concentration of nickel ions was within the range 9–$90\,mg\,l^{-1}$. Tests were also carried out with a supporting electrolyte containing: H_2SO_4 – $130\,g\,l^{-1}$ and $MnSO_4.H_2O$ – $15.5\,g\,l^{-1}$ using aluminium, zinc and nickel substrates (Johnson Matthey). Some experiments indicated below were performed in the absence of $MnSO_4$. All reagents were Merck analytical grade and the solutions were prepared with twice distilled water.

The current-voltage investigations were carried out using glavanostatic and potentiostatic techniques and the electrode impedance was measured within the frequency range 0.03–60 000 Hz at various current or voltage values [13]. The morphology and the surface structure of the deposits was studied with the aid of a Cambridge S250 scanning electron microscope (SEM).

The formation, growth and evolution of hydrogen bubbles on the surface of a stationary cathode (Al "Reidel", containing iron impurities) was investigated *in situ* by optical methods. The specially designed glass cell was equipped with two opposite plane-parallel glass windows for the illumination and photography of the cathode (Fig. 1) using a Zeiss optical microscope at magnifications of 32, 50 and 100.

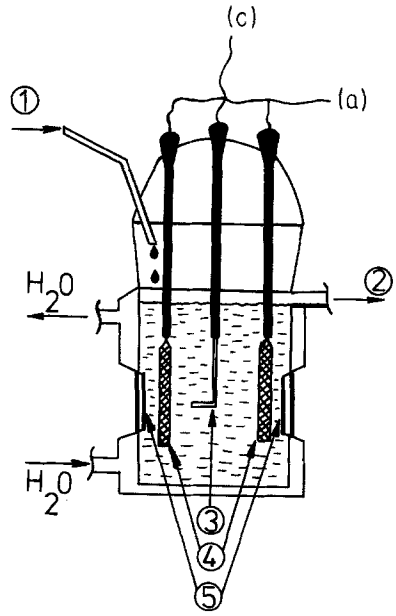

Fig. 1. Laboratory electrowinning cell. (1) Solution feeder; (2) Cell overflow, (3) Aluminium cathode, (4) Pb (1% Ag) anodes, (5) Plane – parallel glasses; (A) Anode; (C) Cathode.

3. Results and discussion

3.1. *Stationary polarization curves*

Figure 2 shows a series of galvanostatic polarization curves obtained with different electrodes. Curve 1 was obtained with a zinc electrode, formed after depositing zinc at $I = 5\,A\,dm^{-2}$ for 1 h in the base electrolyte. Curves 2, 3 and 4 were obtained under identical conditions, but in an electrolyte containing $9\,mg\,l^{-1}$ nickel ions, after 1, 3 and 6 h respectively. Curves 5, 6 and 7 were obtained in the supporting electrolyte containing $9\,mg\,l^{-1}$ nickel ions with aluminium, zinc and nickel cathodes, respectively, in an effort to investigate the rate of hydrogen ion discharge in the absence of zinc ions.

The results shown in Fig. 2 suggest:

(i) When no nickel ions are present in the electrolyte, the polarization curve is relatively stable with time, retaining its shape even after 6 h, with well separated anodic and cathodic regions corresponding to the irreversible zinc-redox reaction.

(ii) In the presence of $9\,mg\,l^{-1}$ nickel ions, the polarization curve 2 gradually, but in a definite way, shifts to more positive potentials as time elapses (curves 3 and 4).

(iii) Curves 5, 6 and 7 provide evidence that the rate of hydrogen evolution is slowest on a zinc cathode, while the nickel electrode shows an enhanced depolarization of this process by 0.4 V with respect

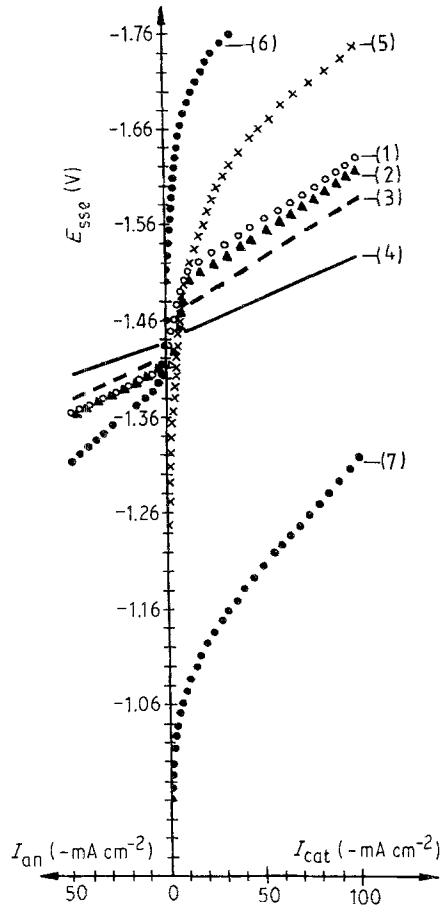

Fig. 2. Galvanostatic polarization curves obtained at $\omega = 2000$ rpm.

to aluminium and 0.6 V as compared with zinc (at $I = 5\,A\,cm^{-2}$). This is naturally a consequence of the difference in the hydrogen ion discharge mechanism on these substrates [14, 15].

Therefore, the progressive depolarization of the cathodic process with time in the presence of nickel ions (curves 2, 3 and 4 in Fig. 2) occurs as a result of both an increase in the cathode roughness as time elapses and the catalytic effect of nickel, codeposited with zinc, in enhancing the hydrogen evolution rate.

3.2. *Electrode impedance during zinc deposition*

An example of a complex plan impedance diagram obtained in the absence of Ni^{2+} ions is shown in Fig. 3. Three inductive loops can be observed below

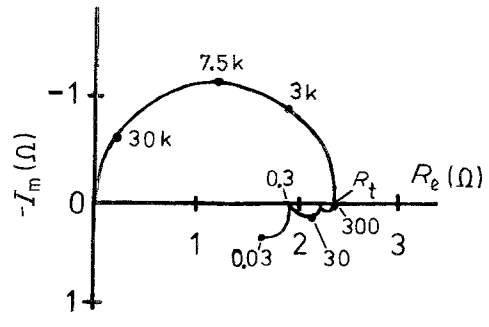

Fig. 3. Complex impedance diagram $Z = R - jG$ corresponding to curve 1 in Fig. 2 at $i = 50\,mA\,cm^{-2}$.

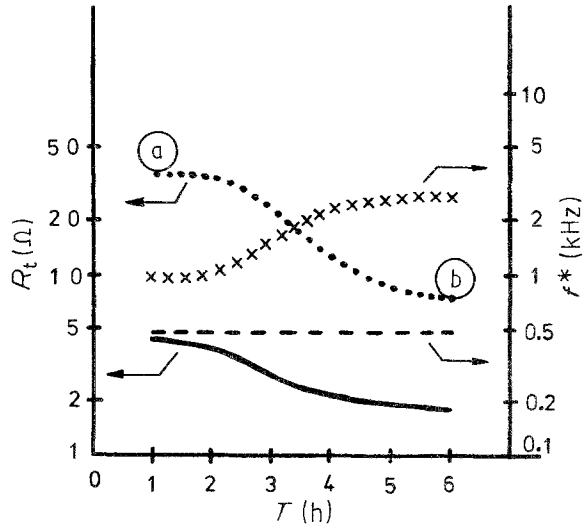

Fig. 4. Time-dependence of R_t and f^* at $i = 50\,mA\,cm^{-2}$: R_t (——), f^* (– – –); and at $i = 0$: R_t (· · · ·), f^* (xxx).

300 Hz, in agreement with the low frequency relaxation processes already reported in slightly acidic sulphate electrolytes [16] and related to the presence of absorbates on the electrode. In the present case of highly acidic solutions where hydrogen evolution occurs with zinc deposition (the metal deposition yield is approximatively 90–94%) the lowest frequency considered was 0.03 Hz, so as to avoid the stray-fluctuations of the alternating response of the system due to bubble formation on the electrode.

During the initially stable regime observed in the presence of Ni^{2+} ions the same type of impedance diagram was obtained, showing clearly the existence of two inductive loops at frequencies higher than 0.3 Hz. During the potential decrease, the enhanced bubble formation reduced the reliable frequency domain down to approximatively 1 Hz. By contrast, the potential shift seemed to be associated with changes in the parameter of the high frequency capacitance loop ascribed to the charge transfer resistance R_t in parallel with the double layer capacitance C_{dl}. The variation of R_t and the frequency f^* at the apex of the capacitance loop: $f^* = (2\pi R_t C_{dl})^{-1}$ are given against time (Fig. 4). For the current density of $50\,mA\,cm^{-2}$, R_t decreased, whereas f^* remained time-independent, in agreement with an increase in the surface area due to a progressively roughened electrode. When the electrode was polarized at the corrosion potential ($i = 0$) after various periods, t, of metal deposition, f^* was observed to increase with time, thus indicating, not only an increased surface area, but also an enhanced electrode reactivity, possibly due to the progressive accumulation of deposited nickel on the electrode surface.

3.3. *Simulated destabilization of the electrode potential*

In order to clarify the mechanism by which the codeposited nickel acts, experiments were carried out in which, at a certain stage of zinc deposition, the

electrode surface was treated by deposition of a nickel layer in a supplementary cell, followed by zinc deposition. During these experiments the change in the electrode potential was continuously monitored as a criterion for the state of the electrode surface.

In the absence of Ni^{2+} ions in the primary cell utilized for zinc deposition, the state of the electrode was destabilized at will by depositing a nickel layer in a secondary cell, after a fixed duration, $t = 1$ h, of zinc deposition. The nickel was deposited from an electrolyte containing: 0.01 M $NiSO_4$, 1 M Na_2SO_4, 0.2 M NaCl and 0.5 M H_3BO_3 at the potential -1.56 V/SSE chosen so as to correspond to the conditions for stable zinc deposition. At this potential, nickel deposition occurred under diffusion control in such a dilute electrolyte, at a rate corresponding to the limiting current density $I_l = 2FD_{Ni}C_{Ni}/\delta$. With a disc electrode rotated at $\omega = 100$ rpm, δ is close to 50 μm in aqueous medium with $D_{Ni} = 10^{-5}$ cm^2 s^{-1} and with the kinematic viscosity, $\nu = 10^{-2}$ cm^2 s^{-1}. Consequently, at a limiting current density of 3.8 mA cm^{-2}, nickel deposited on a zinc electrode for 4.5 s in the secondary cell was equivalent to about 30 monolayers. On returning the electrode to the primary cell so that zinc deposition occurred again, the electrode potential immediately shifted from -1.54 V/SSE to -1.42 V/SSE which is very close to the Zn corrosion potential in this solution. Moreover, at the same time the transfer resistance was also reduced thus indicating that the electrode state had been immediately changed in a manner equivalent to the shift which was taking place slowly from point (a) to point (b) in Fig. 4.

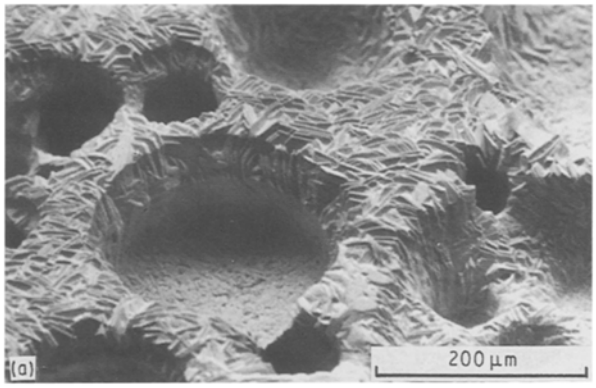

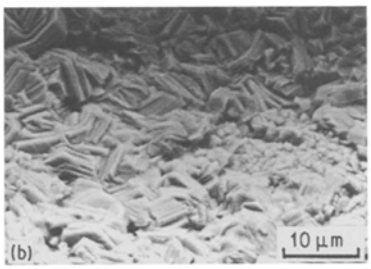

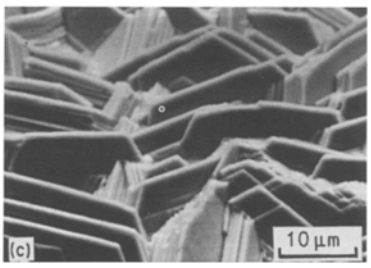

Fig. 5. SEM microphotographs of a Zn deposit obtained from a base electrolyte at $i = 50$ mA cm^{-2} and $\omega = 2000$ rpm after 60 minutes electrolysis time: (a) general view, (b) at the bottom of holes, (c) at the flat surface (outside of the holes).

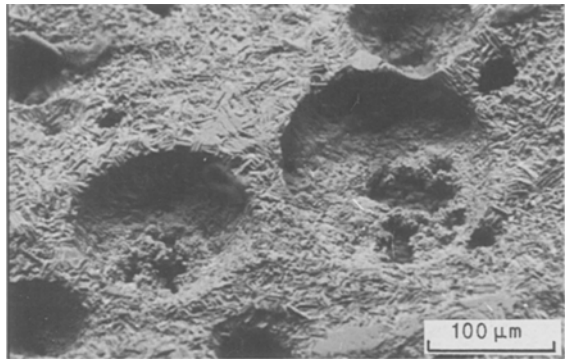

Fig. 6. SEM micrographs of a Zn deposit obtained from a base electrolyte containing 9 mg l^{-1} Ni ions at $i = 50$ mA cm^{-2} and $\omega = 2000$ rpm after 90 minutes electrolysis time.

3.4. *Electrode morphology*

Under steady conditions, without Ni^{2+} ions in the electrolyte, numerous holes of different sizes, corresponding to the formation of bubbles, appeared on the deposit (Fig. 5a). The existence of holes, whose depth is close to the zinc deposit thickness, indicates that the bubbles were formed and developed at specific places on the electrode surface from the beginning of the electrolysis. In addition it was observed at higher magnification that the size of zinc crystals, composed of hexagonal platelets, increased with increasing time, as evident from a comparison of crystals at hole bottoms (Fig. 5b) to those on the flat surface (Fig. 5c).

After zinc deposition for 90 min in the presence of Ni^{2+} ions in the electrolyte, corrosion features are visible on the electrode mostly in the holes (Fig. 6). Some cracks or pits also appear at the bottom of holes where the deposit was completely dissolved down to the Al substrate. Consequently, the areas where hydrogen had evolved appear to have been preferentially corroded. A similar phenomenon was observed immediately following the formation of the nickel layers in the secondary cell, subsequently to zinc deposition for 30 min in the primary cell containing the Ni^{2+} free electrolyte.

3.5. *Influence of the hydrodynamic conditions*

With increasing rotation speed, ω, hydrogen bubbles are more frequently removed and renewed on the electrode surface as suggested in Fig. 7. As a consequence the deposit appears to be more regular at high rotation speeds (Fig. 7a) and the rotating disc electrode does not favour the electrode destabilization. It is noteworthy that without $MnSO_4$ in the electrolyte (Fig. 7a), the number of bubble holes is much lower than in Fig. 5a obtained in the presence of

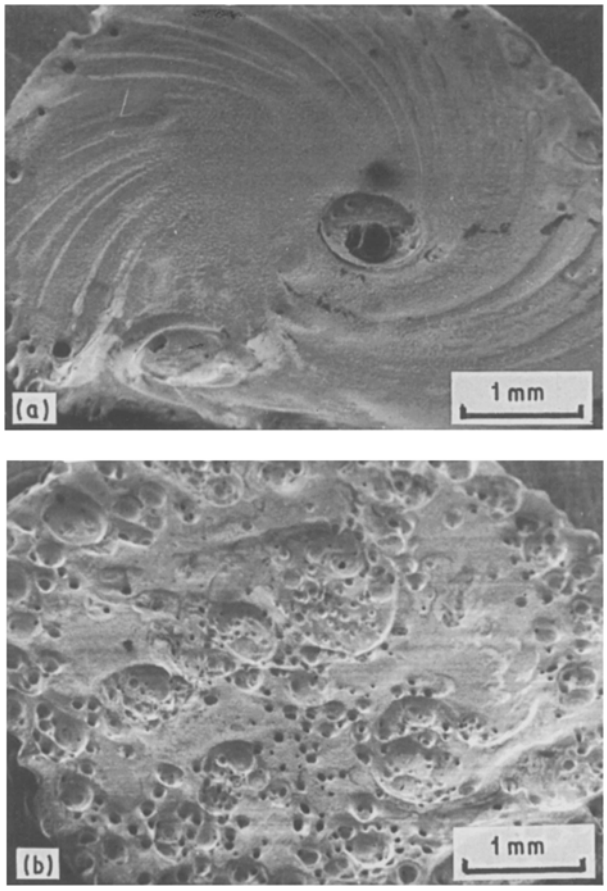

Fig. 7. SEM microphotographs of a Zn deposit obtained from a base electrolyte (without Mn) containing 9 mg l^{-1} Ni ions at i = 50 mA cm^{-2} and different rotation speeds: (a) ω = 2500 rpm, (b) ω = 100 rpm. Electrolysis time: 90 min.

$MnSO_4$; this compound undoubtedly enhances the hydrogen evolution reaction.

The electrode destabilization is much more easily produced when using a vertical electrode partially insulated with a heat shrinkable inert tube (Fig. 8a).

As shown in Fig. 9, the insulated cylinder appears to favour the electrode destabilization which occurs after 8 minutes for ω = 0 and 20 minutes for ω = 2000 rpm. The presence of the insulator appears to

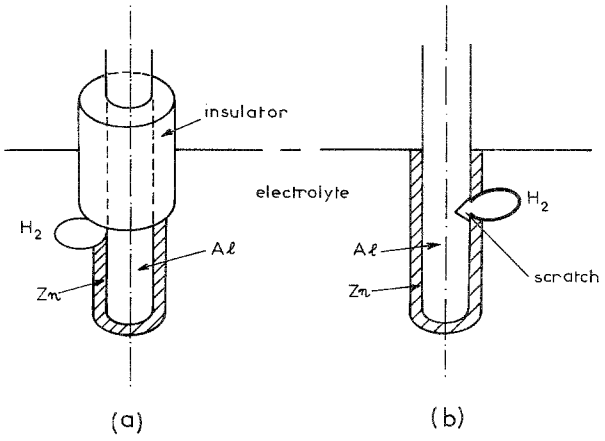

Fig. 8. Schematic representation of the vertical Al electrode insulated with a heat-shrinkable inert tube (a) or scratched before deposition (b).

favour the attachment of large bubbles at the metal/insulator border.

The electrode destabilization is indeed very sensitive to the presence of a defect favouring the bubble attachment: either the presence of the insulator, which retains the bubbles (Fig. 8a), or the existence of a scratch (Fig. 8b) produced with a cutter on the Al substrate. At the same time the electrode destabilization is correlated with a significant increase in the charge transfer resistance, R_t, consistent with an enhanced screening effect of bubbles. As a matter of fact, with no insulator and with a properly polished electrode (emery paper grade 1200), the electrode potential remains stable (Fig. 9, Curve 4). Under the same electrolyte and current density conditions, the potential of a rotating disc electrode remains stable for (at least) one hour.

The relationship between the electrode impedance and the electrode destabilization appears more clearly after a number of cycles corresponding to successive zinc deposition and 'self-dissolution' of the zinc deposit. From Fig. 10 it can be seen that the dissolution of zinc deposit is systematically accompanied by an increase in both the charge transfer resistance,

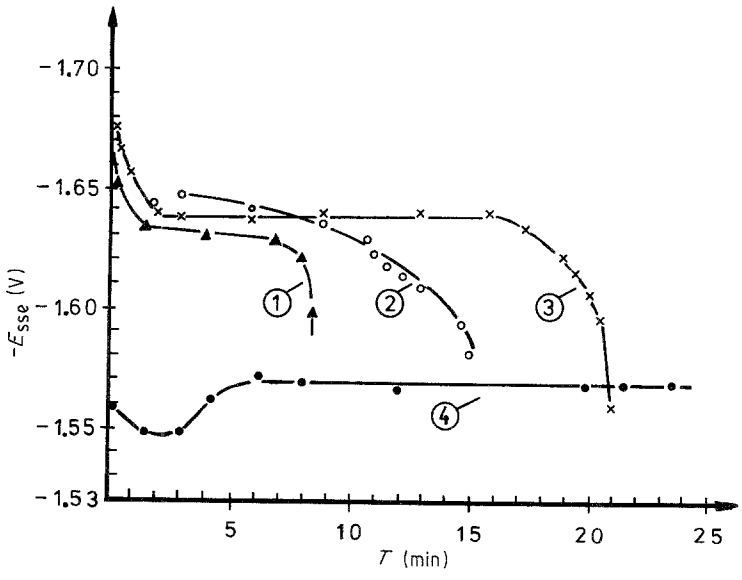

Fig. 9. Galvanostatic potential time curves obtained with an insulated vertical electrode at i = 50 mA cm^{-2} an different rotation speeds: (1) ω = 0 rpm, (2) ω = 1000 rpm, (3) ω = 2000 rpm, (4) ω = 1000 rpm; Al cathode without insulating inert tube. Same electrolyte as for Fig. 7.

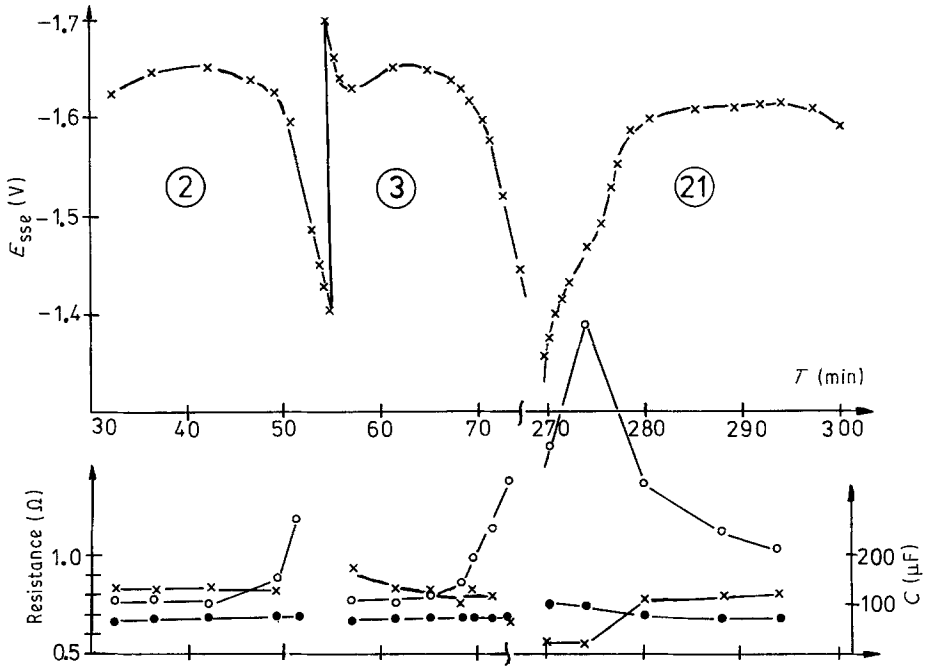

Fig. 10. Time-dependence of; (○) transfer resistance R_t, (●) electrolyte resistance R and (x) electrode capacitance C during 5 hour deposition at rotation speed $\omega = 0$ rpm. Cycles deposition/dissolution are numbered: 2, 3, . . . 21. Same electrolyte as for

R_t, and the electrolyte resistance, R, and also with a decrease in the electrode capacitance, C. All these variations reflect the screening effect of bubbles during zinc 'self-dissolution'.

With increasing number of cycles, the shape of the potential cycle is modified: the time necessary for the electrode to recover the zinc deposition potential (about -1.64 V/SSE) becomes longer, probably because of a progressive accumulation of nickel nuclei and surface defects on the electrode. The SEM photograph of the electrode after cycle 21 (Fig. 11) shows that the Al substrate is progressively corroded. In addition, the EDAX analysis of the stripped electrode after cycle 21 reveals the presence of nickel in the corrosion holes of the Al substrate.

3.6. *Optical (in situ) studies of the electrode surface*

With the aid of the cell presented in Fig. 1 it was possible to observe the initiation and growth of hydrogen bubbles up to their separation from the electrode surface. The L-shaped stationary cathode offered the possibility of investigating these processes simultaneously upon the horizontal and vertical parts of the cathode.

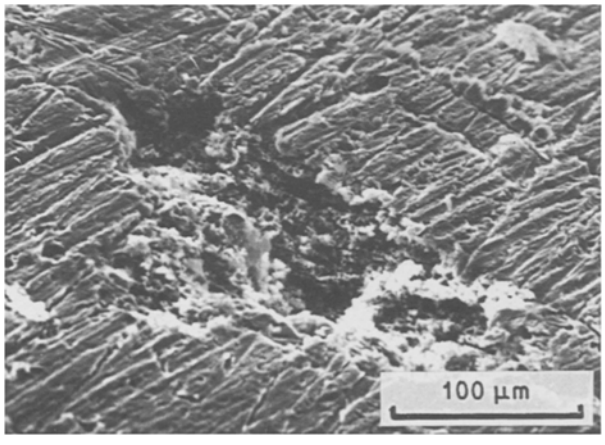

Fig. 11. SEM micrograph of the Al cathode just after electrode destabilization following the cycle 21.

In both the base electrolyte and the Ni^{2+} containing solution, the hydrogen bubbles remain on the cathode for relatively long periods (approximately 5–10 minutes) because the electrolyte slowly enters and leaves the cell in a laminar flow mode, simulating the conditions during zinc electrowinning.

The photographs of bubbles were used for the evaluation of both the wetting angle, θ, between the gaseous and solid phases, as well as the mean height of the hydrogen bubbles. It was established that in the presence of Ni^{2+} both the wetting angle and the mean height of bubbles increase with time during the 'induction period' (Fig. 12). In addition, the wetting angle is higher than in the base electrolyte. In the presence of Ni^{2+}, the observations also provide evidence that there are specific sites on the electrode surface which generate relatively big hydrogen bubbles with high wetting angles (Fig. 13). Obviously these observations lead to the conclusion that the 'induction period' should be related to the renewal of these big bubbles, which can screen the electrode during their residence time on the cathode.

4. Physical model of the 'induction period'

4.1. *Theoretical background*

It is well known from the investigations of gas evolution processes on electrodes and their wetting by the electrolyte, that the equilibrium state of a gas bubble on a solid surface is essentially determined by the action of two forces: capillary (F_c) and hydrostatic (F_h) [17]. The first force, acting along the attachment perimeter of the bubble, F_c, is equal to the product of

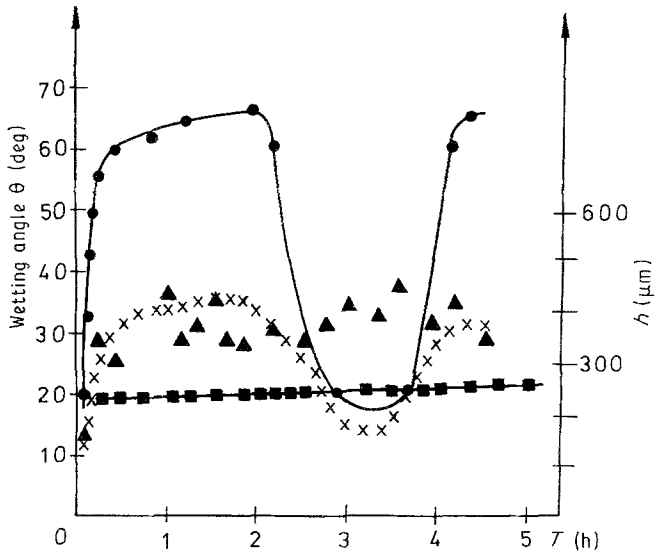

Fig. 12. Time-dependence of the wetting angle θ and mean height h of the hydrogen bubbles formed on a stationary Al cathode. Base electrolyte: θ (■), h (▲); and base electrolyte with 9 mg l^{-1} Ni ions: θ (●), h (x).

the value of this perimeter (πd) and the vertical component of the surface tension (σ) between the solution and the gas phase [18] (Fig. 14). Thus

$$F_c = \pi d \sigma_{23} \sin \theta \quad (1)$$

where

$$\cos \theta = \frac{\sigma_{13} - \sigma_{12}}{\sigma_{23}} \quad (2)$$

The strength of the hydrostatic buoyant force, F_h, lifting the gas bubble in the liquid can be determined by Archimedes law

$$F_h = Vqg \quad (3)$$

It is important to remark that Equation (3) does not take into account the term related to the curvature forces and is only a first approximation.

It has been unambiguously established [19] that the gas bubble is separated from the electrode surface when the forces F_c and F_h become equal, a situation reached for the critical size of the bubble. According to Equations (1) and (3) the size of the gas bubble which can remain attached to the electrode surface is an increasing function of θ.

A characteristic feature in the case of gas evolution upon electrically charged metal surfaces is the fact that the value of σ_{12} changes with the electrode potential [20], or more precisely with its charge, in a manner similar to that of the electrocapillary curves, i.e. σ_{12} acquires its maximum value at the zero charge potential of the electrode [17, 21]. Therefore it can be concluded that the maximum size bubbles (maximum θ) can remain attached to the cathode at the zero charge potential. Higher anodic or cathodic polarizations cause a decrease in the size of the gas bubbles, regardless of the nature of the gas [17].

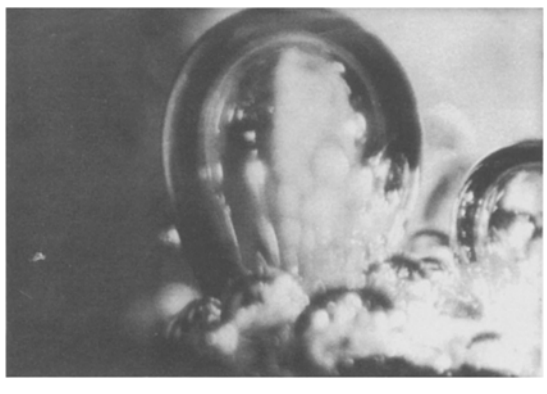

Fig. 13. A photograph of bubbles formed after 90 min deposition in the presence of 9 mg l^{-1} Ni ions. Magnification ×100.

4.2. *Discussion of the experimental results:*

In our opinion, the explanation of the phenomenon, of the induction period can be related to the hydrogen bubble formation stage on the active regions of the cathode surface, containing codeposited nickel. The model for the development of the pitting defect with the participation of a hydrogen bubble is illustrated in Fig. 15.

The locally codeposited nickel depolarizes the hydrogen evolution rate considerably at some active sites. This leads to the initiation and development of hydrogen bubbles, with a high wetting angle, up to a size which depends on the electrode potential.

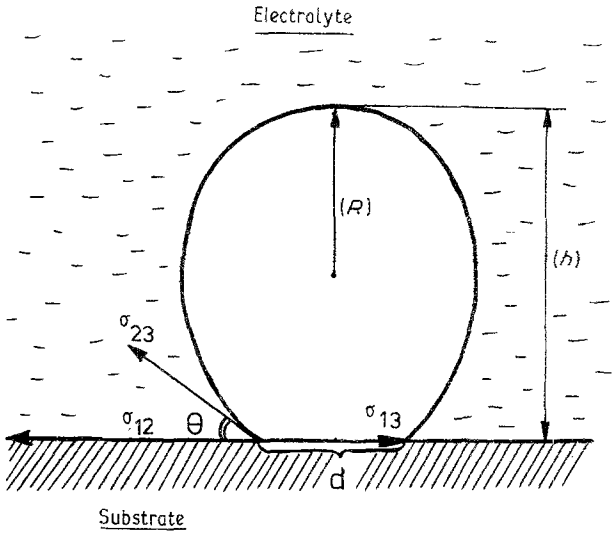

Fig. 14. Equilibrium state of a gas bubble upon a solid surface.

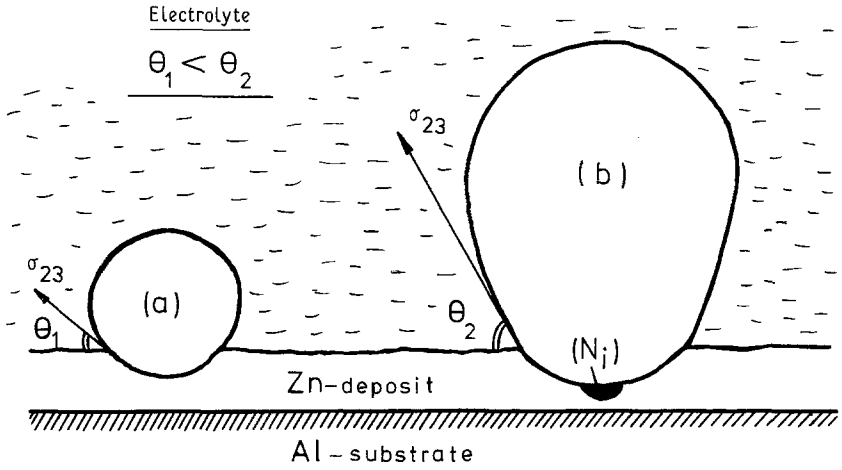

Fig. 15. Schematic representation of the 'screening effect' of the hydrogen bubbles generated: (a) on Zn; (b) on codeposited Ni.

Later, quite large hydrogen bubbles develop on certain nickel-rich sites (Fig. 13) which completely screen the codeposited nickel from the bulk electrolyte (Fig. 15). Then, by nullifying the external current at the site of the gas bubble, a 'local galvanic cell' (zinc/nickel) with e.m.f. about 0.5 V is formed at this site and the 'self-dissolution' of zinc starts at the bottom of the hydrogen bubble (Fig. 6). This process is further amplified by the fact that the zinc electrode should then be locally polarized at its corrosion potential, approximatively equal to the zero charge potential of zinc [22]. As indicated in the theoretical part, gas bubbles at E_{zc} have the maximum size, probably enhancing their screening effect.

It can be conceived that the presence of iron impurities in the Al substrate, which catalyses the discharge rate of hydrogen ions similarly to nickel, favours the formation of big hydrogen bubbles early during zinc deposition and thereby decreases the induction time.

The influence of the hydrodynamic conditions is also consistent with the model of bubbles resident on the electrode surface. By decreasing the electrolyte movement, the residence time of bubbles on the electrode surface increases, thus facilitating their growth and leading to a reduced induction time for the electrode destabilization.

The use of some surface active agents in zinc electrowinning practice, for example, bone-glue, foaming preparations, etc, for the decrease, or partial elimination of the deleterious effect of the metallic impurities can also be easily explained on the basis of the model. It is well known that absorbed surface active agents considerably decrease the surface tension on the metal/electrolyte interface [18]. In addition, many surface active agents increase the cathodic overvoltage of zinc deposition [3, 5, 23]. The combination of the two effects can lead to the formation of smaller hydrogen bubbles which are more easily separated from the cathode surface.

5. Conclusion

As a result of detailed voltammetric, impedance, electron microscopic and optical investigations of the peculiarities encountered in zinc electrowinning from nickel-containing sulphuric acid electrolytes, a model of the explanation of the 'induction period' has been proposed and its dependence on the process conditions elucidated. The model is based on the screening effect of hydrogen bubbles formed on the nickel-rich regions on the cathode, which are isolated from the bulk electrolyte. It was shown that at the bottom of hydrogen bubbles, the zinc corrosion potential is reached, which enhances the formation of hydrogen bubbles with a maximum wetting angle, corresponding to a maximum screening effect.

The proposed model was then used for the explanation of the effect of different parameters including hydrodynamic conditions and the presence of surface active agents on the duration of the 'induction period'.

Acknowledgement

The authors are grateful to Professor M. Froment (LP15 du CNRS, France) for valuable discussion of the experimental results throughout this work.

References

[1] U. Turomshina and V. Stender, *J. Appl. Chem.* USSR **28** (1955) 372, **28** (1955) 447.
[2] D. Fosnach and T. O.'Keefe, *J. Appl. Electrochem.*, **10** (1980) 495.
[3] M. Jaksic, *Surf. Technology*, **24** (1985) 95, **28** (1986) 113, **29** (1986) 95.
[4] M. Maja and P. Spinelli, *J. Electrochem. Soc.*, **118** (1971) 1538.
[5] D. Mackinnon, J. Brannen and P. Fenn, *J. Appl. Electrochem.*, **17** (1987) 1129.
[6] D. Mackinnon, R. Morrison and J. Brannen, *J. Appl. Electrochem.*, **16** (1986) 53.
[7] M. Maja, N. Penazzi, R. Fratesi and G. Roventi, *J. Electrochem. Soc.*, **129** (1982) 2695.
[8] Yar-Ming Wang, T. O'Keefe and W. James, *J. Electrochem. Soc.*, **127** (1980) 2589.
[9] R. Fratesi, G. Roventi, M. Maja and N. Penazzi, *J. Appl. Electrochem.*, **10** (1980) 765.
[10] I. Wark, *J. Appl. Electrochem.*, **9** (1979) 721.
[11] I. Gamali, F. Danilov and V. Stender, *J. Appl. Chem.*, USSR, **36** (1963) 337.
[12] G. Znamenskiy and B. Bezjazikov, *J. Appl. Chem.*, USSR, **38** (1965) 361.
[13] C. Gabrielli, 'Identification of electrochemical processes by frequency response analysis, Technical Report no 004/83, Solarton Instruments (1984).

[14] N. Shohoji, *Surf. Technology*, **28** (1986) 365.
[15] S. Trassati, *Z. für Phys. Chem.* N.F., **98** (1975) 75.
[16] I. Epelboin, M. Ksouri and R. Wiart, *J. Electrochem. Soc.*, **122** (1975) 1206.
[17] A. Frumkin, Electrochemical Processes, Nauka Press, Moscow (1987) p. 171.
[18] R. Johnson and R. Dettre, 'Wettability and Contact Angles – Surface and Colloid Science', (Edited by E. Matijevic and F. Eirich), Wiley-Jutersc. New York, (1969), p. 85.
[19] B. Kabanov and A. Frumkin, *J. Phys. Chem.*, USSR, **4** (1933) 538; **165** (1933) 433.
[20] N. Brandon and G. Kelsall, *J. Applied Electrochemistry*, **15** (1985) 475; **15** (1985) 485.
[21] A. Frumkin, A. Gorodezkaja, B. Kabanov and N. Nekrassov, *J. Phys. Chem.*, USSR, **3** (1932) 351; **4** (1933) 529.
[22] D. Dobos, 'Electrochemical Data', Mir Press, Moscow (1980), p. 249.
[23] B. Lamping and T. O'Keefe, *J. Metal. Trans.*, **7B** (1976) 551.
[24] I. Kiriljus, Electrochemical Hydrogenation, Nauka Press, Alma-Alta (1981), p. 23.